Ocean Engineering 142 (2017) 125–132

Contents lists available at ScienceDirect

Ocean Engineering

journal homepage: www.elsevier.com/locate/oceaneng

Dam break flow solution using artificial neural network

Omid Seyedashraf[a], Abbas Rezaei[b], Ali Akbar Akhtari[c,*]

[a] Department of Civil Engineering, Kermanshah University of Technology, Kermanshah, Iran
[b] Department of Electrical Engineering, Kermanshah University of Technology, Kermanshah, Iran
[c] Department of Civil Engineering, Razi University, Kermanshah, Iran

ARTICLE INFO

Keywords:
Artificial neural network
Dam break flow
Shock waves
Shock dominated flow
Saint-Venant equations

ABSTRACT

The ability of a mathematical model to simulate the dam break shock-wave and rarefaction wave propagation is beneficial in the context of modeling shock dominated engineering problems. In this study, a novel technique based on artificial neural network (ANN) along with an equation is proposed and detailed for the solution of the one-dimensional dam break problems without source terms. The research is motivated by the fact that the classic numerical models show severe oscillations in the results, besides; all the existing analytical solutions are complex piecewise functions. Accordingly, a quick solution with a single equation and smooth results can be helpful for analyzing the problem. The model is developed with five parameters consisting the channel length, upstream and downstream water depths, time, and the distance factors as the input data, while the water depths and flow velocities are considered as the outputs. The model is well validated against several numerical and analytical solutions. Findings indicate that the ANN is capable of simulating the dam break flow problem satisfactorily and that the proposed model has outperformed the classical numerical results while its CPU time is one-third that of the numerical scheme.

1. Introduction

Dam break shock-wave is the flow emanating from the sudden release of an initially stationary water body. When a dam is broken, the impounded water flees through the opening into the downstream river. In these circumstances, the probability of loss of lives and properties is much intensive, since the warning time necessary to reach the people living in the downstream region is too short. The existence of more than 800,000 dams and kilometers of dykes in the world makes it more interesting for engineers to address the issue. Accordingly, the need to have a real-time flood zoning prediction and warning system is critical to make logical decisions necessary to evacuate areas prone to inundations. On the other hand, from the mathematical point of view, in numerical simulation of the shock waves and rarefaction waves induced by dam break flows, shock fronts have been characterized as sudden discontinuities with rapid variations of flow velocity and water depth. These two issues are the main difficulties in the numerical simulation of these flows.

Concerning the complex dynamics of dam break flows, the numerical simulation of the respective flows requires advanced mathematics. The importance of the topic primarily comes from its application in mathematical modeling of the shock dominated problems (Boulahia et al., 2014; Brouwer et al., 2015; Inage et al., 2013). The need for such models has prompted and maintained the development of the finite-difference method (FDM) (Luo and Gao, 2015; Ouyang et al., 2014), finite-volume method (FVM) (Aureli et al., 2008; Stecca et al., 2015; Zhang et al., 2014), and the finite-element method (FEM) (Isakson et al., 2015; Ortiz, 2014; Seyedashraf and Akhtari, 2017; Triki, 2013) to solve the relevant governing equation systems. These developments include the so-called shock-capturing techniques, i.e. the Total-variation-diminishing and Flux-corrected-transport schemes (Boulahia et al., 2014; Kuzmin et al., 2005; Ortiz, 2014; Toro, 2001) to improve the accuracy of the models. However, considering the simultaneous solution of the continuity, momentum and energy equations, and the number of iterations required to achieve convergence, numerical methods are computationally expensive (Malekmohamadi et al., 2008).

Taking inspiration from the application of artificial neural networks (ANNs) in various areas of hydraulics and ocean engineering (Emiroglu et al., 2011; Hooshyaripor et al., 2014; Kişi, 2008; Makarynskyy, 2004; Malekmohamadi et al., 2011; Sun et al., 2014), and the analytical solution of the dam break problems in verifying numerical models (Chanson, 2008, 2009; Hunt, 1983; Jain, 2001; Mangeney et al., 2000; Martins et al., 2016; Ritter, 1892; Stoker, 1992), the aim of this study is to develop a new concept for dam break flow predictions. The procedure is a regular ANN model trained by a significant number of input data obtained from Stoker's analytical solution. As a validation of

* Corresponding author.
E-mail addresses: o.seyedashraf@kut.ac.ir, o.seyedashraf@gmail.com (O. Seyedashraf), a.rezaee@kut.ac.ir (A. Rezaei), akhtari@razi.ac.ir (A.A. Akhtari).

http://dx.doi.org/10.1016/j.oceaneng.2017.07.002
Received 8 June 2016; Received in revised form 30 June 2017; Accepted 1 July 2017
Available online 05 July 2017

Nomenclature

b	Bias term
f	Activation function of the hidden layers
g	Gravity
h	Water depth
h_L	Water depth in the upstream channel
$_{hR}$	Water depth in the downstream channel
n	Manning's roughness coefficient
O_g	ANN output
S	Topographical and frictional source terms
S_b	Depth changes
S_f	Friction
s	Bore speed
T	Time
T_c	ANN output
U	Matrix of variables
U_i	ANN output
u	Depth-integrated velocity in the x- directions
X	X-direction space
x	ANN inputs
Yj	ANN output
W	Weighting factor

the proposed technique, the obtained results are compared with the analytical and classical numerical methods. Despite its simplicity, the approach is quick and accurate. Moreover, unlike other analytical piecewise-defined equation systems, this study presents a general monolithic equation for quick solution of the problem (Stoker, 1992).

This paper is organized as follows. In Section 2, the mathematical theory of the Saint-Venant equations (SVEs) is described, in Section 3, the required input and output data for the ANN model are presented, and in Section 4, the model is explained. Subsequently, in Section 5, the computed water depth and flow velocity results are shown, and finally, in Section 6 the findings of the study are summarized.

2. Saint-Venant equations

Most of the analytical solutions of the one-dimensional dam break flows are founded on the SVEs, which are based on the assumption of the hydrostatic pressure and Boussinesq approximations. Consequently, a pair of coupled partial differential equations expressed by two variables representing the flux vectors describes the flow characteristics (Sheu and Fang, 2001):

$$U_T + F_X + S = 0 \tag{1}$$

in which U represents the solution vector of the conservative variables, F is the flux vector, and S accounts for the topographical and frictional source terms, while T and X denote the partial derivatives regarding time and space, respectively.

$$U = \begin{Bmatrix} h \\ uh \end{Bmatrix} \tag{2}$$

$$F = \begin{Bmatrix} uh \\ u^2h + gh^2/2 \end{Bmatrix} \tag{3}$$

$$S = \begin{Bmatrix} 0 \\ gh(S_b - S_f) \end{Bmatrix} \tag{4}$$

in which u is the depth-integrated velocity component and h is water depth. S_b is defined by the depth gradients while S_f corresponds to friction.

$$S_f = \frac{n^2 u(u^2 + v^2)^{1/2}}{h^{4/3}} \tag{5}$$

where n represents the manning's roughness coefficient.

In this study, the above-mentioned equations are not solved directly, and the homogeneous case is considered.

3. Input and output data

Twenty-four test cases with varied upstream (H_0) and downstream (H_1) water surface levels were examined in the experiments. Table 1 summarizes the test cases and the considered H_0-H_1 water levels.

Stoker's linear interval equation system was formulated and solved in MATLAB to generate the required input and output data (Stoker, 1992).

$$u(X,T) = \begin{cases} 0 & if \quad X < \frac{L}{2} - T\sqrt{gh_L} \\ \frac{1}{3T}(2(X + T\sqrt{gh_L}) - L) & if \quad \frac{L}{2} - T\sqrt{gh_L} \le X \le (u_2 - c_2)T + \frac{L}{2} \\ u_2 & if \quad (u_2 - c_2)T + \frac{L}{2} < x \le sT + \frac{L}{2} \\ 0 & if \quad X > sT + \frac{L}{2} \end{cases} \tag{6}$$

$$h(X,T) = \begin{cases} h_L & if \quad X < \frac{L}{2} - T\sqrt{gh_L} \\ \frac{1}{9g}(2\sqrt{gh_L} - \frac{1}{2T}(2X - L))^2 & if \quad \frac{L}{2} - T\sqrt{gh_L} \le X \le (u_2 - c_2)T + \frac{L}{2} \\ \frac{h_R}{2}\left(\sqrt{1 + \frac{8s^2}{gh_R}} - 1\right) & if \quad (u_2 - c_2)T + \frac{L}{2} < X \le sT + \frac{L}{2} \\ h_R & if \quad X > sT + \frac{L}{2} \end{cases} \tag{7}$$

in which u_2 and c_2 parameters are described as follows:

$$u_2 = S - \frac{gh_R}{4S}\left(1 + \sqrt{1 + \frac{8s^2}{gh_R}}\right) \tag{8}$$

$$c_2 = \sqrt{\frac{gh_R}{2}\left(\sqrt{1 + \frac{8s^2}{gh_R}} - 1\right)} \tag{9}$$

where s is the bore speed, the positive root of $(u_2 + 2c_2 - 2\sqrt{gh_L})$, L is the length of the flow region, h_L and h_R are the water depths at the left- and right-hand sides of the dam.

The layout of the initial condition is shown schematically in Fig. 1.

4. Artificial neural network

The ANN systems are typical non-mechanistic models for modeling

Table 1
The considered H_0-H_1 water levels for the ANN data train- testing.

Case	1	2	3	4	5	6	7	8	9	10	11	12	13	14	15	16	17	18	19	20	21	22
H_0	10	8	9	7	9	7	30	40	50	10	11	15	18	50	6	40	30	20	60	13	10	20
H_1	5	1	6	2	5	3	3	5	7	1	6	8	5	12	1	4	10	7	7	5	2	3

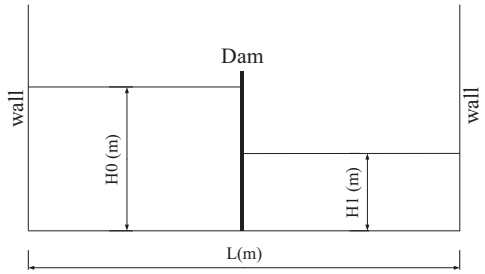

Fig. 1. Scheme of the initial conditions for the dam break problem.

complex systems in approximation problems such as medicine, finance, and engineering (Hornik et al., 1989; Taylor, 1996). The advantage of ANN is its high precision capability to predict untrained data. Moreover, it can be used to model and predict the data, which tend to be ignored by statistical methods.

Multi-layer perceptron (MLP) networks (Hornik, 1991), which are the most widely used ANNs, have minimum three layers; namely, the input, hidden and output layers. Each layer consists of the basic processing elements in the ANNs called neurons. The synapses of the biological neurons are modeled in the ANNs as weights. Here, an accurate model based on the MLP is used. The input parameters are the length of the domain (L), the water depth in the upstream section of the dam (H_0), the water depth in the downstream section (H_1), distance (X), and time (T). On the other hand, the water depth (H) and flow velocity (U) are considered as outputs.

The data set was obtained by solving Stoker's equation system and was divided into two sets. One set, about 70%, for training the ANN model, and about 30% for testing the trained network. The MATLAB 7.0.4 software was used to train and test the proposed model. To acquire the best ANN model, a training process algorithm was employed, which is shown in Fig. 2. In this figure, the mean absolute error (MAE) is given by the following equation:

$$MAE = \frac{1}{N}\sum_{i=1}^{N} |X_i(An) - X_i(\mathrm{Pred})| \tag{10}$$

in which 'X *(An)*' and 'X (*Pred*)' are the analytical and ANN results, respectively. Here, N is the total number of data.

To acquire the best model with minimum error for the outputs H and U, various ANN structures with a different number of hidden layers (from 1 to 4), different number of neurons in each hidden layer (from 1 to 12), different number of epochs (from 50 to 750) and various types of training algorithms (including: Trainlm, Traingda, Trainbfgc, Trainoss, Traingdx, Traingdm, Traincgf, Traincgp, Trainbfg, Trainrp, Traingdm, Trainbr, Trainr, Trainb and Traingd algorithms) were trained and tested. The training process algorithm shown in Fig. 2 is described below:

The training and testing data were selected and the initial parameter values for MAEo (the MAE obtained for the best ANN model), MAEn (the MAE obtained for the current ANN model), number of epochs, type of training algorithm, number of hidden layers and number of neurons in each hidden layer were chosen. Subsequently, each ANN network with the selected parameters was trained and tested with the respective training and testing data. The MAEn was calculated. Accordingly, for MAEn < MAEo (the current ANN network is better), the best earlier ANN model was replaced with the current ANN network, and its parameters were saved. This process was repeated for all possible ANN networks while changing the parameters (the number of hidden layers, number of neurons in each hidden layer, number of epochs and types of training algorithm) for each new ANN model. At the end of this process, the best ANN network was obtained (Fig. 3).

The output from ith neuron in the first hidden layer is as follows:

$$U_i = f\left(\sum_{k=1}^{5}(x_k W_{ki}) + b_i\right) \qquad i = 1, 2, ..., 10 \tag{11}$$

In the second hidden layer, the output of the jth neuron can be obtained by:

$$Y_j = f\left(\sum_{k=1}^{10}(U_k W_{kj}) + b_j\right) \qquad j = 1, 2, ..., 9 \tag{12}$$

The output of the cth neuron in the third hidden layer is given by:

$$T_c = f\left(\sum_{k=1}^{9} Y_k W_{kc} + b_c\right) \qquad c = 1, 2, .., 10 \tag{13}$$

Finally, in the output layer, the output of the gth neuron is given by the following equation:

$$O_g = \sum_{k=1}^{10}(T_k W_{kg}) + b_g \quad g = 1, 2 \tag{14}$$

in which x, b and W stand for the inputs, bias term and weighting factor, respectively. Moreover, f is the activation function of the hidden layers. The obtained ANN model has one output layer with five neurons, three hidden layers with 10, 9 and 10 neurons in the first, second and third hidden layers, respectively, and one output layer with 2 neurons. The model structure has the following specifications: learning rate=0.5, obtained the number of epochs=250, Trainlm as the training algorithm and Tansig function as the activation function for the hidden layers, where, the Tansig function for variable X is given by:

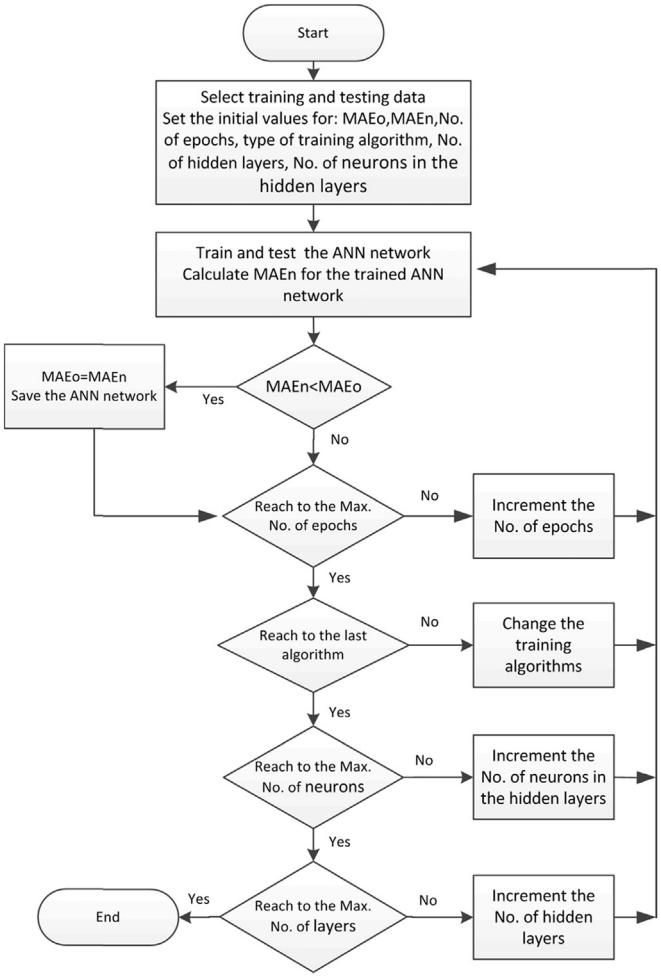

Fig. 2. The training process algorithm to obtain the best ANN model.

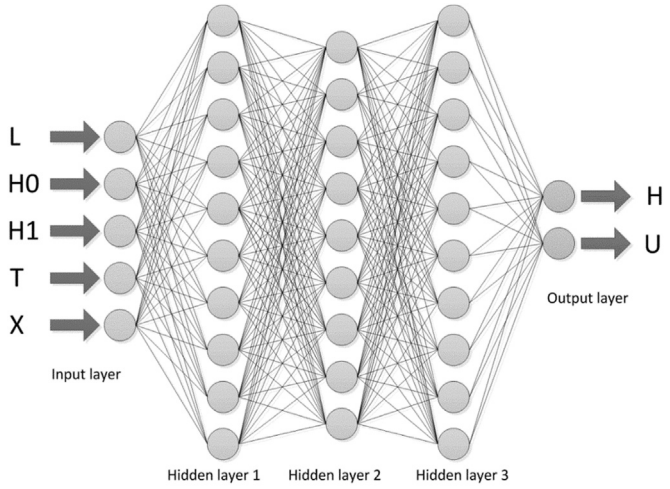

Fig. 3. The proposed ANN model.

$$\text{Tan } sig(X) = \frac{2}{1 + e^{-2X}} - 1 \tag{15}$$

5. Results and discussion

To examine the performance of the proposed model, the predictions were compared with the known analytical data. The obtained ANN (MLP) results are shown in Fig. 4, where the correlation factor (CF) is calculated by:

$$CF = 1 - \left[\frac{\sum_{i=1}^{N} (X_i(An) - X_i(\text{Pred}))^2}{\sum_{i=1}^{N} (X_i(An))^2} \right] \tag{16}$$

According to Fig. 4, it is clear that the predicted water depths are close to the analytical data. This shows the ability of ANN as a reliable model to predict shock dominated complex hydraulic problems.

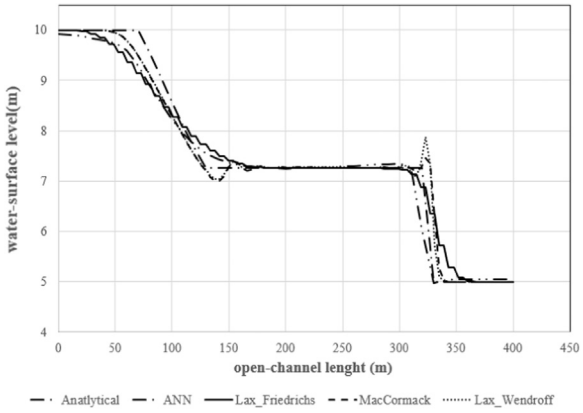

Fig. 5. Comparison of the water surface levels for the analytical, numerical (FDM), and ANN dam break predictions ($H_0 = 10m$, $H_1 = 5m$, $T = 14s$).

In addition to the analytical and ANN simulations, the problem was also numerically solved by three generally used finite-difference schemes; namely, Lax-Wendroff, Lax-Friedrichs, and MacCormack models (LeVeque, 2002). Accordingly, the flow region was discretized into 100 linear computational cells. The results obtained from two tests considering $L = 400m$ and $L = 1200m$ were compared to ANN predictions. The water surface level in the upstream and the downstream sections of the dam for the first and second cases are $H_0 = 10m$, $H_1 = 5m$, and $H_0 = 30m$, $H_1 = 10m$, respectively.

Here, since the flow is transient, solving the SVEs by the FDMs, the time step was obtained according to the Courant-Friedrichs-Lewy (CFL) stability criterion to prevent numerical divergence.

Figs. 5–8 present the obtained numerical, analytical and ANN results for the test cases.

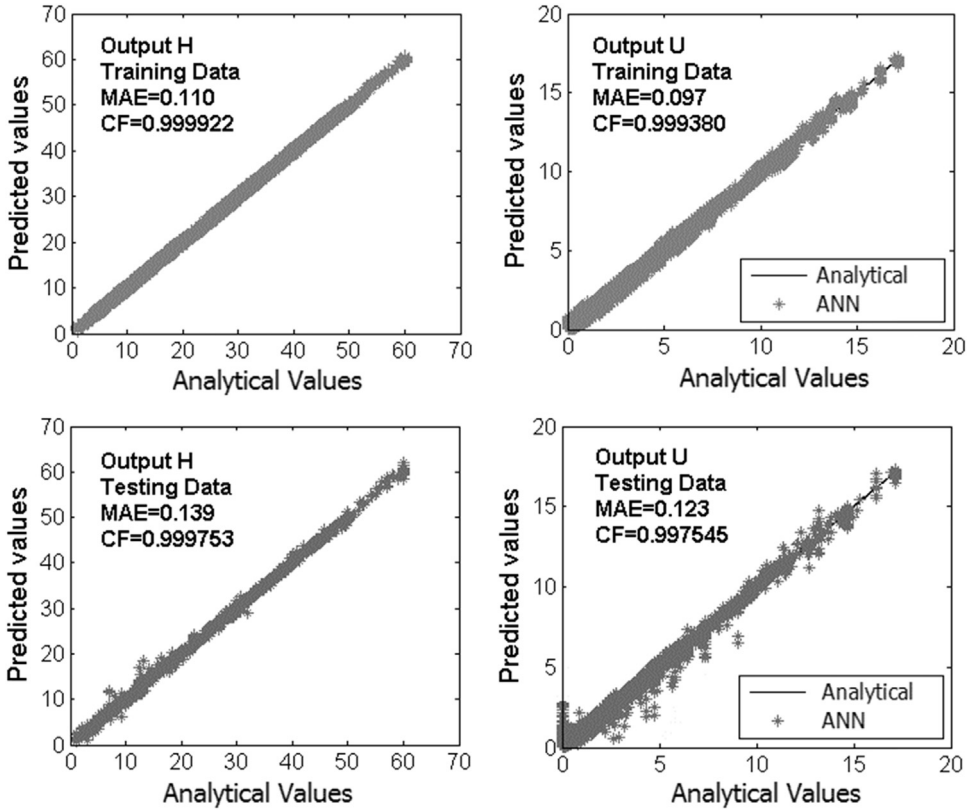

Fig. 4. Comparison of the analytical and ANN results for training and testing data.

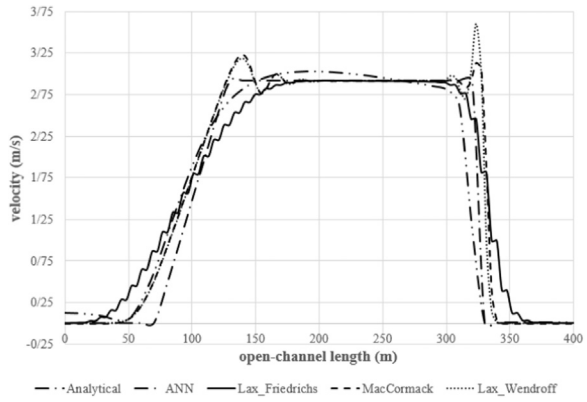

Fig. 6. Comparison of the flow velocities for the analytical, numerical (FDM), and ANN dam break predictions ($H_0 = 10m$, $H_1 = 5m$, $T = 14s$).

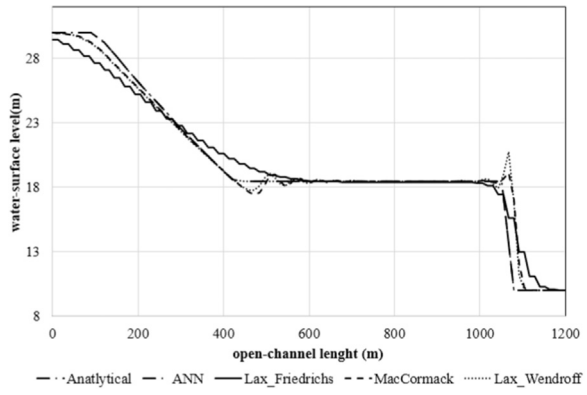

Fig. 7. Comparison of the water surface levels for the analytical, numerical (FDM), and ANN dam break predictions ($H_0 = 30m$, $H_1 = 10m$, $T = 30s$).

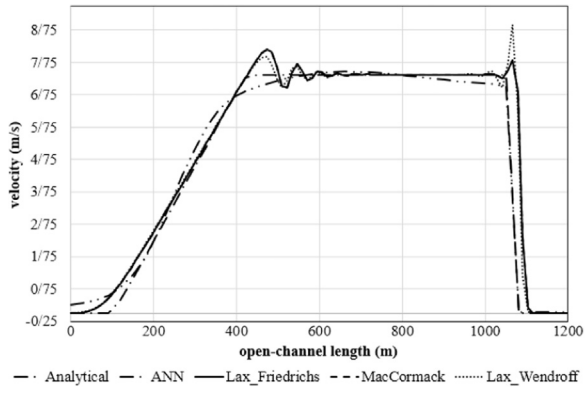

Fig. 8. Comparison of the flow velocities for the analytical, numerical (FDM), and ANN dam break predictions ($H_0 = 30m$, $H_1 = 10m$, $T = 30s$).

Table 2
Comparison of the *MAE* and *CF* measures for the ANN and numerical predictions.

	Lax-Wendroff	Lax–Friedrichs	MacCormack	ANN
MAE (L = 400)	0.165	0.180	0.176	0.155
CF (L = 400)	0.984	0.983	0.982	0.987
MAE (L = 1200)	0.325	0.769	0.409	0.257
CF (L = 1200)	0.989	0.984	0.989	0.998

Figs. 6 and 8 confirm the results associated with Figs. 5 and 7 showing that the model outperforms the classical methods and has a shock-capturing capability.

Table 3
MAE and *CF* measures for the ANN results.

H_1/H_0	0.278	0.117	0.100	0.167	0.200	0.500	0.333
MAE	0.069	0.248	0.359	0.120	0.088	0.155	0.257
CF	0.9996	0.9997	0.9990	0.9992	0.998	0.987	0.998

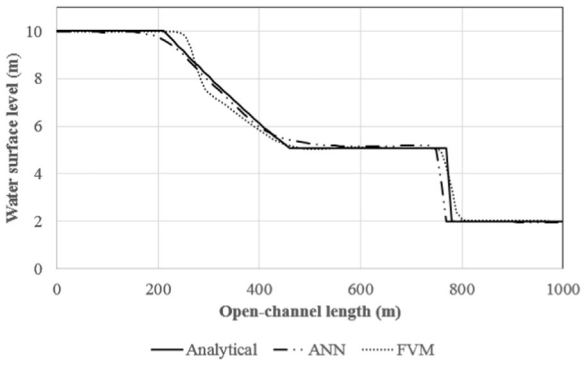

Fig. 9. Comparison of the water surface levels for the analytical, Ying et al. (2004)'s finite volume model, and ANN dam break predictions ($H_0 = 10m$, $H_1 = 2m$, $T = 30s$).

It is clear that all the naive finite difference based numerical models produce spurious fluctuations in the flow conditions near the abrupt changes of water depths, where the ANN model presents smooth results. The measuring factors for the predicted results in the first and second dam-break benchmarks are $MAE = 0.155$, $CF = 0.987$ and $MAE = 0.257$, $CF = 0.998$, respectively. Table 2 compares the *MAE* and *CF* measures for the ANN, Lax-Wendroff, Lax–Friedrichs, and MacCormack predictions in both test cases.

On a Pentium 4 operating at 2.2 GHz and 3 gig RAM, it took about 4.81 s to complete the computations for Stoker's piece-wise equation systems. Moreover, for the numerical (FDM) and ANN models with the same system configuration, it took 8.09 and 2.36 s, respectively. This shows that the ANN model performs at least two and three times faster than the numerical and analytical model.

The proposed model is also compared against an upwind conservative finite volume model with a weighted average water-surface-gradient approach. In this test case, the considered flow region is $1000m$ long rectangular channel. The dam is located at $500m$ from the downstream end of the channel. Initially, the downstream water level is $2m$ and the upstream depth is $10m$. The $H_1/H_0 = 0.2$ ratio was picked to investigate the performance of the scheme for flow transition prediction from the sub- to supercritical flow regimes, which is difficult for naive numerical methods. Ying et al. (2004) tested this benchmark to examine a finite volume method.(Table 3)

Fig. 9 represents the computed ANN, FVM and analytical results at $30s$ after the dam failure.

Fig. 9 depicts the existence of nonphysical water depth data near $300m$ before the dam in Ying et al. (2004)'s FVM results. However, the flow conditions are well covered by the ANN model and the shock waves, especially the rarefaction wave, are predicted without spurious fluctuations with the calculated MAE and CF measures of 0.088 and 0.998, respectively.

The analytical and ANN solutions of the water surface level and flow velocity for four other tests with different initial conditions are shown in Figs. 10–13.

According to the obtained MAE and CF measures of the predicted results, the proposed model shows to be able to predict the shock-wave front and rarefaction formation precisely for both the sub- and supercritical dam-break flow regimes. Comparing to the naive FDMs and FVMs, the proposed ANN model is able to produce results for the

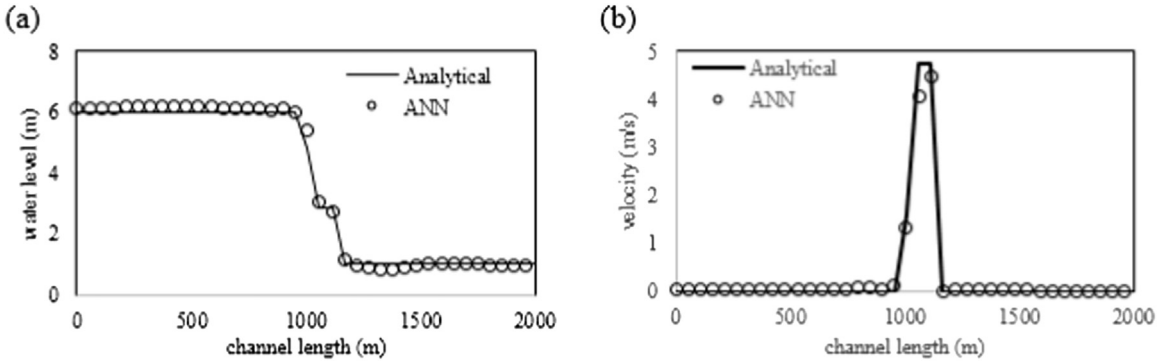

Fig. 10. Comparison of the analytical and ANN dam break flow simulation ($H_0 = 6m$, $H_1 = 1m$, $T = 11s$), (a) Water depth, (b) Flow velocity.

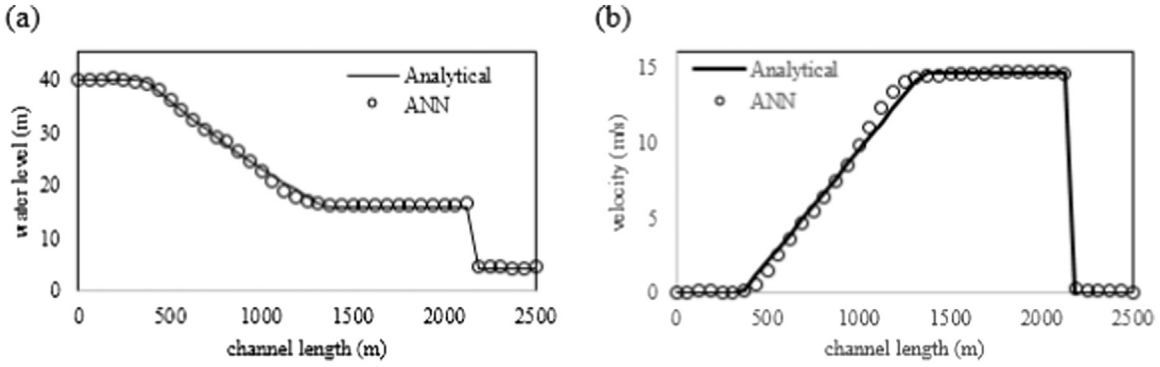

Fig. 11. Comparison of the analytical and ANN dam break flow simulation ($H_0 = 40m$, $H_1 = 4m$, $T = 46s$), (a) Water depth, (b) Flow velocity.

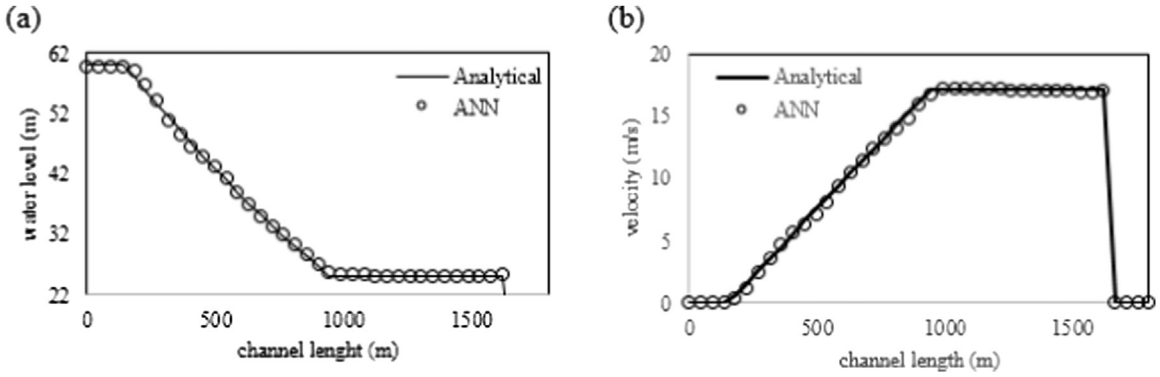

Fig. 12. Comparison of the analytical and ANN dam break flow simulation ($H_0 = 60m$, $H_1 = 7m$, $T = 32s$), (a) Water depth, (b) Flow velocity.

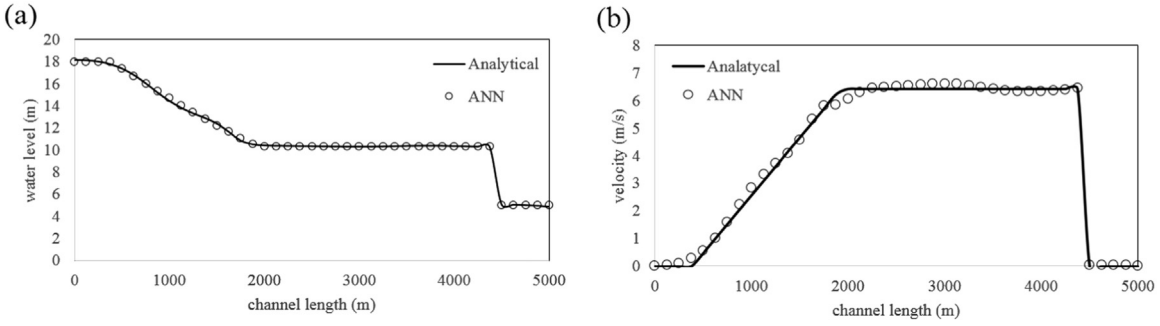

Fig. 13. Comparison of the analytical and ANN dam break flow simulation ($H_0 = 18m$, $H_1 = 5m$, $T = 160s$), (a) Water depth, (b) Flow velocity.

Table 4
The obtained equation for the outputs H and U using the best proposed ANN model.

Y1=Tansig(−0.003198*L-0.038934*H1−0.0035341*H0+0.13516*T+0.0063427*X +1.0953);
Y2=Tansig(−0.00098261*L+0.053067*H1−0.040447*H0−0.013338*T +0.001965*X+0.16564);
Y3=Tansig(0.0024285*L+0.043279*H1−0.044447*H0−0.019659*T-0.0047199*X-0.13386);
Y4=Tansig(−4.9199e-007*L-0.0025926*H1+0.010203*H0−1.5062e-005*T +2.7711e-006*X-0.11956);
Y5=Tansig(−0.00056667*L-0.0026436*H1+0.023968*H0−0.0033995*T +0.0012824*X-2.4659);
Y6=Tansig(−0.060515*L-0.0031838*H1−7.4756*H0−2.2005*T+0.17765*X-7.4842);
Y7=Tansig(6.3985e-005*L+0.13765*H1−0.027028*H0+0.00075949*T-0.00015341*X-0.7389);
Y8=Tansig(−0.00064443*L+0.16155*H1−0.031594*H0+0.02043*T+0.0012931*X-0.034484);
Y9=Tansig(0.0018214*L-0.0085783*H1−0.0099791*H0+0.075948*T-0.0037111*X+0.6893);
Y10=Tansig(0.11617*L-0.31063*H1−0.47722*H0+0.30365*T+0.039732*X +1.4839);
Z1=Tansig(0.025728*Y1−0.0032256*Y2+0.062246*Y3−6.0333*Y4+0.17087*Y5+0.026296*Y6+ 0.043153*Y7+ 0.02752*Y8−0.060688*Y9+0.38763*Y10−1.2638);
Z2=Tansig(0.0042598*Y1−0.0092435*Y2+0.0077661*Y3−4.3411*Y4+0.005326*Y5+0.091902*Y6+ 0.0048469*Y7+0.026831*Y8−0.013263*Y9+1.87*Y10+0.078782);
Z3=Tansig(1.2073*Y1−0.90289*Y2−2.5144*Y3+4.4573*Y4+1.3711*Y5+2.4481*Y6+0.19907*Y7+ 0.22638*Y8−1.0683*Y9−0.92654*Y10−0.96092);
Z4=Tansig(−0.077806*Y1+0.013572*Y2−0.18786*Y3−1.0519*Y4−0.086145*Y5−0.02455*Y6−0.83021*Y7−0.26913*Y8+0.047125*Y9+0.73155*Y10+ 0.26759);
Z5=Tansig(−3.5136*Y1−0.48892*Y2+0.15383*Y3−2.8414*Y4−0.23332*Y5+0.60949*Y6+2.6973*Y7−1.3688*Y8+0.86124*Y9+2.1704*Y10+2.352);
Z6=Tansig(3.9348*Y1+0.37711*Y2−0.13354*Y3+2.2893*Y4+0.15909*Y5−0.83624*Y6−3.6735*Y7+ 1.6218*Y8−1.1872*Y9−3.0908*Y10+ −2.1755);
Z7=Tansig(2.3471*Y1−25.6676*Y2+19.2569*Y3+5.6946*Y4+32.8982*Y5−16.5409*Y6+13.9033*Y7−1.5345*Y8+36.7532*Y9+3.4642*Y10+4.9331);
Z8=Tansig(25.0932*Y1+1.3265*Y2−1.2607*Y3−1.8804*Y4+4.535*Y5+4.0937*Y6−0.32924*Y7+ 3.5075*Y8−11.4712*Y9−3.693*Y10+ −2.2828);
Z9=Tansig(−1.2688*Y1−0.09041*Y2+1.185*Y3+1.913*Y4+0.2619*Y5+0.17292*Y6+4.0433*Y7−0.037983*Y8+0.0022147*Y9+2.041*Y10+3.4058);
W1=Tansig(−4.6535*Z1−2.0023*Z2−0.38357*Z3−5.4567*Z4+2.3593*Z5+2.2197*Z6+1.0728*Z7+ 0.10757*Z8−2.1345*Z9+0.04915);
W2=Tansig(−1.865*Z1−1.4759*Z2+0.28448*Z3−2.6134*Z4+1.9394*Z5+0.79875*Z6−0.84321*Z7+ 1.5607*Z8−0.98937*Z9+ −0.94721);
W3=Tansig(−0.21033*Z1−0.54818*Z2−0.0083537*Z3−1.3217*Z4−0.18508*Z5−0.18944*Z6−0.0066432*Z7+ 0.00023985*Z8+0.1118*Z9+ 1.5786);
W4=Tansig(1.1595*Z1+1.2205*Z2−0.15985*Z3+0.12488*Z4+0.0048132*Z5+0.23049*Z6−2.4765*Z7+0.37312*Z8+0.80648*Z9+ 2.4861);
W5=Tansig(−0.50784*Z1+4.6097*Z2−1.2944*Z3−0.51299*Z4−0.94935*Z5−0.70611*Z6−11.0323*Z7+ 0.22391*Z8+0.51628*Z9+ 4.6173);
W6=Tansig(2.6205*Z1+0.92303*Z2−0.62352*Z3+0.69654*Z4−3.8297*Z5−2.8864*Z6+1.7457*Z7+ 2.2065*Z8+0.65909*Z9+ 2.4697);
W7=Tansig(−3.0175*Z1−0.84867*Z2−0.36559*Z3+0.60621*Z4−0.33367*Z5−0.090784*Z6−8.2836*Z7+ 0.45595*Z8+0.34122*Z9+ 5.2753);
W8=Tansig(4.3564*Z1−0.78114*Z2−3.2156*Z3+2.8689*Z4−3.9836*Z5−3.5548*Z6−11.5873*Z7−1.1206*Z8+ 1.2898*Z9+10.5258);
W9=Tansig(−3.3094*Z1+3.6162*Z2+2.1784*Z3+1.6274*Z4−5.6318*Z5−3.4404*Z6−0.49854*Z7+ 0.88488*Z8+0.95545*Z9+ −3.7618);
W10=Tansig(−3.2417*Z1−3.1464*Z2+1.6378*Z3+1.7406*Z4−3.4575*Z5−2.0928*Z6+0.042692*Z7+ 0.9065*Z8+0.96902*Z9+ 1.5074);

specified time rather than solving the governing equation (SVEs) from $t = 0s$ to the specified time (T).

The following single equations have been derived from the proposed dam break water depth and flow velocity.

$$H = |-4.5171 \times W1 - 6.7647 \times W2 + 18.1632 \times W3 - 5.0541 \times W4 - 10.4579 \times W5 - 16.9387 \times W6 + 8.1407 \times W7 + 3.3068 \times W8 - 4.7207 \times W9 + 6.184 \times W10 + 10.8091| \quad (17)$$

$$U = |1.6736 \times W1 + 00.76055 \times W2 - 00.055202 \times W3 - 20.6169 \times W4 - 30.0731 \times W5 + 60.9732 \times W6 + 20.2342 \times W7 - 20.2506 \times W8 + 20.5371 \times W9 - 20.122 \times W10 + 00.73193| \quad (18)$$

where the parameters are summarized in Table 4.

6. Conclusions

In this study, a comprehensive artificial neural network framework was tested on a novel approach to simulate the dam break shock- and rarefaction wave propagation. The following conclusions were derived from the study:

1. Comparisons between the numerical, analytical and ANN predictions revealed that in terms of accuracy, the ANN model has outperformed the classical numerical schemes, and was able to predict the shock-wave front and rarefaction wave formation precisely.
2. The differences between the predictions were found to be similar over the water depth and flow velocity results for six different benchmarks, which show the generality of the developed model.
3. A new equation was proposed to solve the one-dimensional dam break problems. Unlike Stoker's piecewise-defined function (Eqs. 6–9), this study presents the water depth (H) and flow rate (U) in a single monolithic equation as a function of domain-length (L), distance (X), time (T), and water depth (H) in the upstream and downstream sections of the dam.
4. Unlike the numerical models, there is no need to consider the CFL criterion, nor solve the unsteady governing equations from the initial conditions to the desired time. Instead, the proposed equation can be solved for the exact specified time (e.g. $t = 30s$, Fig. 7).
5. According to the obtained measurement accuracy, the model can be used to validate numerical models for the one-dimensional dam break problems without source terms. However, compared to the existing analytical solutions, the proposed technique can be extended to cover different boundary conditions, such as friction, bottom slope, fluid density, etc.
6. Comparing to the numerical and analytical models, the ANN technique is three and two times faster in CPU time, respectively.

Simulations based on the proposed ANN model can be put into practice to study other shock-dominated problems. It is intended for future work to use the proposed model to deal with the two-dimensional dam break and tsunami problems in dry and oblique domains with bottom friction.

References

Aureli, F., Maranzoni, A., Mignosa, P., Ziveri, C., 2008. A weighted surface-depth gradient method for the numerical integration of the 2D shallow water equations with topography. Adv. Water Resour. 31 (7), 962–974.
Boulahia, A., Abboudi, S., Belkhiri, M., 2014. Simulation of viscous and reactive hypersonic flows behaviour in a shock tube facility: TVD schemes and flux Limiters application. J. Appl. Fluid Mech. 7, 2.
Brouwer, K., Crowell, A., McNamara, J., 2015. Rapid Prediction of Unsteady Aeroelastic Loads in Shock-Dominated Flows, In: Proceedings of the 56th AIAA/ASCE/AHS/ASC Structures, Structural Dynamics and Materials Conference, pp. 1–20.

Chanson, H., 2008. A simple solution of the laminar dam break wave. J. Appl. Fluid Mech. 1 (1), 1–10.
Chanson, H., 2009. Application of the method of characteristics to the dam break wave problem. J. Hydraul. Res. 47 (1), 41–49.
Emiroglu, M.E., Bilhan, O., Kisi, O., 2011. Neural networks for estimation of discharge capacity of triangular labyrinth side-weir located on a straight channel. Expert Syst. Appl. 38 (1), 867–874.
Hooshyaripor, F., Tahershamsi, A., Golian, S., 2014. Application of copula method and neural networks for predicting peak outflow from breached embankments. J. Hydro-Environ. Res. 8 (3), 292–303.
Hornik, K., 1991. Approximation capabilities of multilayer feedforward networks. Neural Netw. 4 (2), 251–257.
Hornik, K., Stinchcombe, M., White, H., 1989. Multilayer feedforward networks are universal approximators. Neural Netw. 2 (5), 359–366.
Hunt, B., 1983. Asymptotic solution for dam break on sloping channel. J. Hydraul. Eng. 109 (12), 1698–1706.
Inage, T., Tsuchikura, S., Ota, M., Maeno, K., 2013. Three-dimensional laser interferometric CT (LICT) measurement of shock wave interaction around a circular cylinder. Flow. Meas. Instrum. 31, 102–106.
Isakson, M.J., Chotiros, N.P., Piper, J., 2015. Finite element modeling of propagation and reverberation shallow water waveguide with a variable environment. J. Acoust. Soc. Am. 138 (3), 1898, (1898).
Jain, S.C., 2001. Open-channel Flow. John Wiley & Sons, New York.
Kişi, Ö., 2008. River flow forecasting and estimation using different artificial neural network techniques. Hydrol. Res. 39 (1), 27–40.
Kuzmin, D., Löhner, R., Turek, S., 2005. Flux-corrected Transport: Principles, Algorithms, and Applications 1st ed. Springer, Berlin; New York.
LeVeque, R.J., 2002. Finite Volume Methods for Hyperbolic Problems. Cambridge University Press, Cambridge; New York.
Luo, Z., Gao, J., 2015. The numerical simulations based on the NND finite difference scheme for shallow water wave equations including sediment concentration. Comput. Methods Appl. Mech. Eng. 294, 245–258.
Makarynskyy, O., 2004. Improving wave predictions with artificial neural networks. Ocean Eng. 31 (5–6), 709–724.
Malekmohamadi, I., Bazargan-Lari, M.R., Kerachian, R., Nikoo, M.R., Fallahnia, M., 2011. Evaluating the efficacy of SVMs, BNs, ANNs and ANFIS in wave height prediction. Ocean Eng. 38 (2–3), 487–497.
Malekmohamadi, I., Ghiassi, R., Yazdanpanah, M.J., 2008. Wave hindcasting by coupling numerical model and artificial neural networks. Ocean Eng. 35 (3–4), 417–425.
Mangeney, A., Heinrich, P., Roche, R., 2000. Analytical solution for testing debris avalanche numerical models. Pure Appl. Geophys. 157 (6–8), 1081–1096.
Martins, R., Leandro, J., Djordjević, S., 2016. Analytical solution of the classical dam-break problem for the gravity wave–model equations. J. Hydraul. Eng. 142 (5), 06016003.
Ortiz, P., 2014. Shallow water flows over flooding areas by a flux-corrected finite element method. J. Hydraul. Res. 52 (2), 241–252.
Ouyang, C., He, S., Xu, Q., 2014. MacCormack-TVD finite difference solution for dam break hydraulics over erodible sediment beds. J. Hydraul. Eng. 141 (5), 06014026.
Ritter, A., 1892. Die fortpflanzung de wasserwellen. Z. Ver. Dtsch. Ing. 36 (33), 947–954.
Seyedashraf, O., Akhtari, A.A., 2017. Two-dimensional numerical modeling of dam-break flow using a new TVD finite-element scheme. J. Braz. Soc. Mech. Sci. Eng., 1–9.
Sheu, T.W.H., Fang, C.C., 2001. High resolution finite-element analysis of shallow water equations in two dimensions. Comput. Methods Appl. Mech. Eng. 190 (20–21), 2581–2601.
Stecca, G., Siviglia, A., Blom, A., 2015. An accurate numerical solution to the Saint-Venant-Hirano model for mixed-sediment morphodynamics in rivers. Adv. Water Resour.
Stoker, J.J., 1992. Water Waves; the Mathematical Theory with Applications. Interscience Publishers, New York.
Sun, S., Yan, H., Kouyi, G.L., 2014. Artificial neural network modelling in simulation of complex flow at open channel junctions based on large data sets. Environ. Model. Softw. 62, 178–187.
Taylor, J.G., 1996. Neural Networks and their Applications. UNICOM; Wiley, Chichester; New York.
Toro, E.F., 2001. Shock-capturing Methods for Free-surface Shallow Flows. John Wiley, Chichester; New York.
Triki, A., 2013. A finite element solution of the unidimensional shallow-water equation. J. Appl. Mech. 80 (2), 021001.
Ying, X., Khan, A.A., Wang, S.S., 2004. Upwind conservative scheme for the Saint Venant equations. J. Hydraul. Eng. 130 (10), 977–987.
Zhang, M., Xu, Y., Hao, Z., Qiao, Y., 2014. Integrating 1D and 2D hydrodynamic, sediment transport model for dam-break flow using finite volume method. Sci. China Phys. Mech. Astron. 57 (4), 774–783.